Maximum Flow Routing Strategy with Dynamic Link Allocation for Space Information Networks under Transceiver Constraints

Wei Liu, *Senior Member, IEEE,* Lin Zhu, Huiting Yang, Hongyan Li, *Member, IEEE,* Jiandong Li, *Fellow, IEEE,* Anthony Man-Cho So, *Senior Member, IEEE*

***Abstract*—In this paper, we investigate the maximum flow routing strategy with dynamic link allocation under a constraint on the number of transceivers for space information networks (SINs). Specifically, the time-expanded graph (TEG) is exploited to characterize the dynamic topology of SINs. Furthermore, although there exist multiple feasible links for SINs, only a limited number of them can be actually established due to the constraint on the number of transceivers. Traditionally the established link is fixed within one time interval in the TEG. In order to fully exploit the resource of multiple feasible links, we divide each time interval in the TEG into multiple fine-grained time periods and design the maximum flow routing strategy by jointly optimizing both the fine-grained time period duration and the link allocation as well as the amount of data transmitted on each transmission link and the amount of data stored in each caching link. This problem can be formulated as a mixed-integer quadratic program (MIQP), which is difficult to solve. To overcome this difficulty, we transform the MIQP into an equivalent mixed-integer linear program (MILP), which can be effectively solved by existing methods. Simulation results show that the proposed dynamic link allocation strategy can significantly outperform the fixed link allocation strategy within each time interval.**

***Index Terms*—space information network, time-expanded graph, dynamic link allocation, transceiver constrained, maximum flow**

I. Introduction

Compared with traditional terrestrial networks, space information networks (SINs) have many advantages, such as wide coverage and flexible networking [1]–[4]. Therefore, SINs have attracted intensive research interests [1]–[8]. The SINs usually consist of different types of space platforms, such as geostationary Earth orbit (GEO) satellites, middle Earth orbit (MEO) satellites, low Earth orbit (LEO) satellites, stratospheric balloons, manned and unmanned aircraft, and so on [1]–[3]. Furthermore, the topology of the SINs is dynamic but predictable [8]–[11]. Therefore, the time-varying graphs, such as snapshot graph [9], time-aggregated graph (TAG) [9], [10], [12], and time-expanded graph (TEG) [11], [13], [14], have been widely used to model SINs in order to describe their time-varying characteristics. The snapshot graph uses a series of snapshots to describe the dynamic evolution of the SINs [9]. However, the snapshot graph cannot exploit the storage resource of the node in SINs because there are no connections between snapshots [9], [12]. In contrast, the TEG was proposed to connect the two consecutive snapshots of the same node by caching links, which facilitates the exploitation of the storage of the nodes in the SINs [9], [12].

Recently, maximum flow routing strategies of SINs have received significant attention [10], [12]–[14]. For the maximum flow problem of single commodity dynamic network with constraints on the bandwidth of the transceivers, one routing strategy was proposed in [14]. For the multi-commodity flow problem of single-source-single-sink satellite networks, a STAG-based multiple flow-maximizing routing scheme with delivery delay constraints was proposed in [10]. For the multi-commodity maximum flow of multi-source-multi-sink delay tolerant networks (DTNs), a dynamic combined flow algorithm was proposed in [12] to obtain the maximum flow of two commodities in DTNs.

However, the above-mentioned work on the maximum flow routing strategy does not consider constraints on the number of transceivers. They assume that all feasible links can be established with one time interval.

Different from terrestrial networks, the resources of SINs are more limited due to their size and weight [4], [15]. Therefore, the equipment loaded on the space platforms, such as transceivers, memory, and batteries, is limited [15], [16]. Particularly, only limited number of transceivers can be equipped [16].

Due to constraints on the number of transceivers, not all feasible connections in SINs can be established [5], [8]. Therefore, resource allocation of SINs with constraints on the number of transceivers has attracted intensive research interests [11], [17], [18]. Under constraints on the number of transceivers, a joint scheduling of observation resource and transmission resource based on the event-driven TEG was investigated to meet the diverse service requirements of observation tasks in [11]. Furthermore, under constraints on the number of transceivers, one contact plan strategy based on the extended TEG was proposed to solve the mission aware contact plan problem of coupling multiple time slots [17]. Moreover, under constraints on the number of transceivers,

W. Liu, L. Zhu, H. Yang, H. Li, J. Li are with State Key Labs of Integrated Service Networks, Xidian University, 710071, Xi'an, Shaanxi, P.R. China. Email: liuweixd@mail.xidian.edu.cn; lzhuxd@stu.xidian.edu.cn; htyang0827@stu.xidian.edu.cn; hyli@xidian.edu.cn; jdli@mail.xidian.edu.cn.

A. M.-C. So is with the Department of Systems Engineering and Engineering Management, The Chinese University of Hong Kong, Shatin, N. T., Hong Kong. Email: manchoso@se.cuhk.edu.hk.

The financial support of National Key R&D Program of China (2019YFE0113200), of National Natural Science Foundation of China under Grant (61871452, 91638202, 61931017, 61901317) and of National Key Laboratory of Science and Technology on Communications, UESTC, Chengdu, China, are gratefully acknowledged.

a joint optimization algorithm of the contact plan, power allocation, and mission scheduling based on TEG was proposed in order to achieve fair performance among satellites [18].

However, all existing resource allocation schemes with constraints on the number of transceivers assume that the allocating strategy of the transceiver is fixed within one time interval [11], [17], [18]. That is, once links are established within one time interval, the transceiver cannot be switched to establish other feasible links within one time interval. However, there are generally more feasible links available for transceivers to connect within one time interval than the number of transceivers. Essentially, these feasible links are also one kind of time-varying resources in SINs. Therefore, in order to improve system performance, the transceiver can dynamically switch several times within one time interval to select any feasible link to establish one connection for each time.

Against this background, in this paper We investigate the maximum flow routing strategy with dynamic link allocation within one time interval for SINs for a given time horizon under the constraints on the number of transceivers. Our main contributions are as follows:

1) The TEG is exploited to characterize the dynamic topology of SINs to facilitate the usage of caching links. Furthermore, in order to dynamically allocate the feasible links within one time interval, each time interval of the TEG can be divided into multiple fine-grained time periods. Moreover, for each fine-grained time period, under the constraint of K number of transceivers, only K number of links can be selected from all the feasible links to be established.
2) Under the transceiver constraint, we jointly optimize the fine-grained time period duration and the link allocation as well as the amount of data transmitted on each transmission link and the amount of data stored in each caching link. This problem can be formulated as a mixed-integer quadratic program (MIQP), which is difficult to solve. To overcome this difficulty, we transform the MIQP into an equivalent mixed-integer linear program (MILP), which can be effectively solved by existing algorithms, such as the Branch and Bound algorithm [19, Chapter 11].
3) Simulation results show that under the constraint on the number of transceivers, the proposed dynamic link allocation strategy can significantly outperform the fixed link allocation strategy within one time interval and achieve 12% performance gain.

The rest of the paper is organized as follows. The system model is presented in Section II, while the transceiver constrained maximum flow routing strategy with dynamic link allocation is presented in Section III. In Section IV simulation results are provided to demonstrate the performance of our proposed dynamic link allocation routing strategy, while the conclusion is offered in Section V.

II. SYSTEM MODEL

A. Space Information Network

The SIN considered in this paper includes user satellites, relay satellites, and ground stations [17], [18], [20], as shown in Fig. 1, where user satellites can be observation satellites, space stations, navigational satellites, remote sensing satellites, and so on. The satellites and ground stations in SINs can be considered as nodes in SINs. User satellites can directly transmit the mission data to ground stations when user satellites move into the coverage of the ground stations. Otherwise, user satellites transmit the mission data to ground stations via relay satellites [17], [18], [20]. The transmission of the mission data is shown by the solid line in Fig. 1. The state of connection between nodes in SINs is time-varying and discontinuous. However, as the orbit of the satellite around the earth is periodic, SIN topologies also change periodically and can be predicted [8], [10], [14].

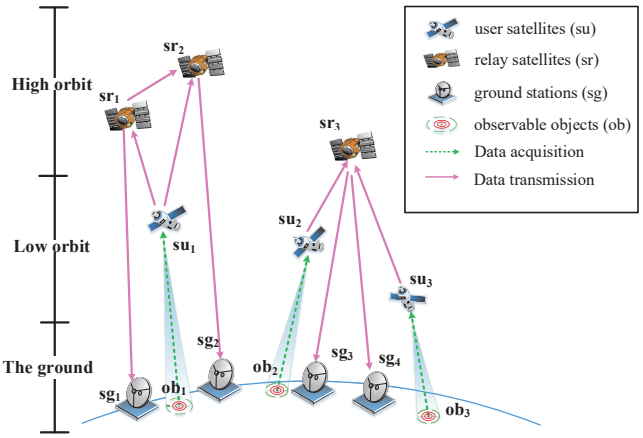

Fig. 1. Schematic diagram of space information network data transmission scenarios.

B. Time-Expanded Graph Model

In this paper, a SIN with H nodes is considered. The i-th node in a SIN is denoted as v_i, for $i = 1, 2, 3, \ldots, H$. Furthermore, for a given time horizon $[0, T)$, it is divided into L time intervals $\{\tau_1, \tau_2, \ldots, \tau_l, \ldots, \tau_L\}$, where τ_l represents the l-th interval, and the length of each time interval is τ. Moreover, we assume that the SIN topology is fixed during the time interval τ and may change at the end of time interval τ. As a result, the highly-dynamic but predictable SIN topology can be described by a TEG $G = (V, E)$ [13], [14], [18], as shown in Fig. 2, where V represents the set of vertices in the TEG G, and E represents the set of edges in the TEG G. Specifically, the vertices and edges can be obtained as follows [13], [14], [18]:

a) Vertices: The vertices in the TEG G correspond to the nodes in SINs and their replica nodes. The set of vertices in the TEG G is denoted as V, which is given by [17]

$$V = \left\{ v_i^l | 1 \le l \le L, 1 \le i \le H \right\}, \tag{1}$$

where v_i^l represents the replica node of the node v_i within the time interval τ_l.

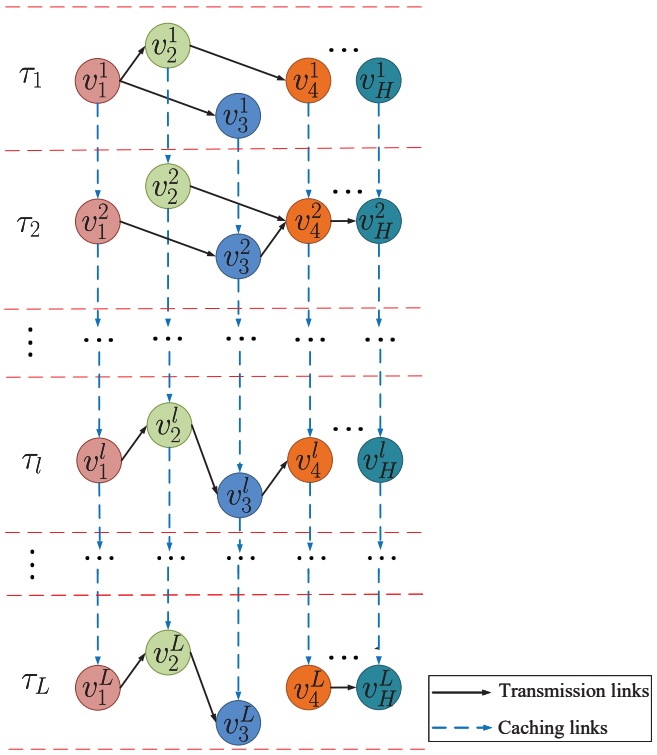

Fig. 2. Time-expanded graph: $G = (V, E)$.

b) Edges: The edges in the TEG G correspond to the links in SINs. The set of edges is $E = E_L \cup E_S$, where E_L is the set of transmission links, while E_S is the set of caching links. When the node v_j^l is in the coverage of the node v_i^l within time interval τ_l, the transmission link from v_i^l to v_j^l is denoted as $\left(v_i^l, v_j^l\right)$, for $i \neq j$. The set of transmission links E_L is given by [13], [17]

$$E_L = \{\left(v_i^l, v_j^l\right) | v_i^l \in V, v_j^l \in V, i \neq j, \\ v_j^l \text{ is in the coverage of the } v_i^l \text{ within time interval } \tau_l\}. \quad (2)$$

The caching link from v_i^l to v_i^{l+1} is denoted as $\left(v_i^l, v_i^{l+1}\right)$, which represents the caching link between two consecutive time intervals τ_l and τ_{l+1} for the node v_i. The set of caching links E_S is given by [13], [17]

$$E_S = \left\{\left(v_i^l, v_i^{l+1}\right) | v_i^l \in V, v_i^{l+1} \in V\right\}. \quad (3)$$

The source node of the TEG G is one of the user satellites, and the destination node is one of the ground stations. Without loss of generality, in the TEG G, the node v_1 is assumed to be the source node, and the node v_H is assumed to be the destination node. The mission flow is transmitted from the source node v_1 to the destination node v_H in SINs within the time horizon $[0, T]$. In this case, all replica nodes of the source node v_1^l, for $l = 1, 2, 3, \ldots, L$, can send data, while all replica nodes of the destination node v_H^l, for $l = 1, 2, 3, \ldots, L$, can receive data.

III. Transceiver Constrained Maximum Flow Routing Strategy with Dynamic Link Allocation

Due to the limited size and weight, each node in SINs can only be equipped with limited number of transceivers [16]. Without loss of generality, in this paper, the number of transceivers of each node is assumed to be K. However, the number of feasible links within one time interval may be more than the number of transceivers of each node K. In this case, not all feasible connections with one time interval can be established, and only k out of all feasible links can be selected to establish K connection at one time instant. Furthermore, in order to dynamically allocate feasible link resources within one time interval, each time interval of the TEG G can be divided into multiple consecutive fine-grained time periods with variable time duration, where the available feasible links are the same for each fine-grained time period within one time interval and transceivers are allowed to switch to establish different connections in different fine-grained time periods.

To this end, each time interval τ_l of the TEG G is divided into N_l consecutive fine-grained time periods, as shown in Fig. 3. The n-th fine-grained time period of τ_l is denoted as $\tau_{l,n}$, for $l = 1, 2, 3, \ldots, N, n = 1, 2, 3, \ldots, N_l$. Furthermore, the length of the $\tau_{l,n}$ is represented by $d_{l,n}$. Therefore, the lengths $\{d_{l,n}\}_{1 \leq l \leq L, 1 \leq n \leq N_l}$ need to satisfy the following constraint

$$\sum_{n=1}^{N_l} d_{l,n} = \tau. \quad (4)$$

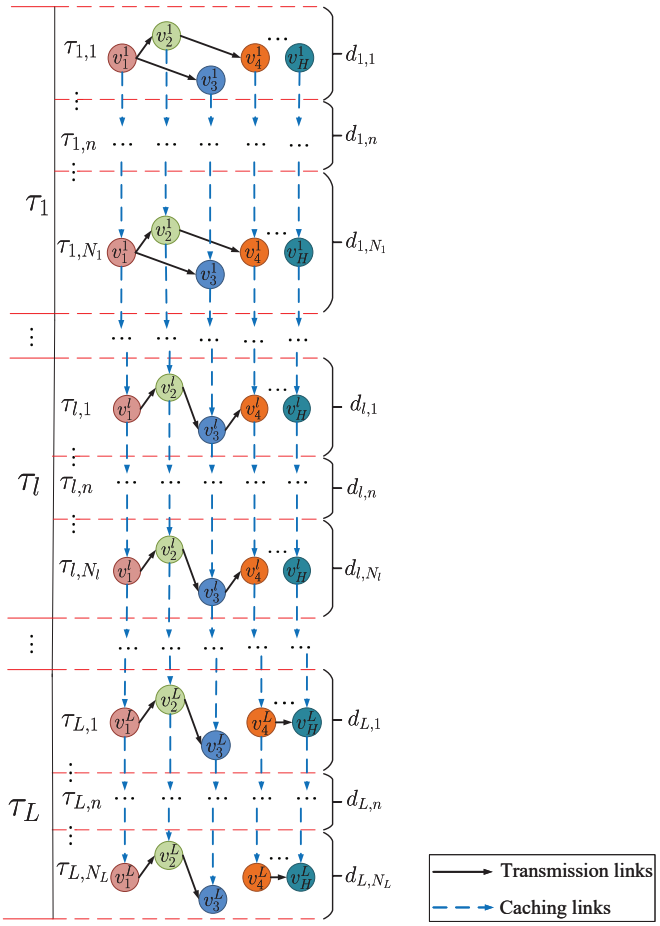

Fig. 3. Time-expanded graph for dynamic link allocation within one time interval.

Furthermore, the indicator of whether transmission link

$\left(v_i^l, v_j^l\right)$ is established at $\tau_{l,n}$ is denoted as a binary variable $g_{\tau_{l,n}}^{\left(v_i^l, v_j^l\right)}$, i.e.,

$$g_{\tau_{l,n}}^{\left(v_i^l, v_j^l\right)} = \begin{cases} 1 \text{ , if node } v_i^l \text{ is connected to node } v_j^l \\ \quad \text{within the fine-grained time period } \tau_{l,n} \\ 0 \text{ , otherwise.} \end{cases} \tag{5}$$

A. Transceiver Constraints

For the node v_i^l, as only K transceivers are equipped, this node can only send data to at most another K nodes within each fine-grained time period $\tau_{l,n}$ [11], i.e., the number of transmission links coming out of the node v_i^l must be less than or equal to K. Thus, the following constraint must be satisfied [11]

$$\sum_{\left\{v_j^l:\left(v_i^l, v_j^l\right)\in E_L\right\}} g_{\tau_{l,n}}^{\left(v_i^l, v_j^l\right)} \leq K. \tag{6}$$

Furthermore, the node v_i^l can only receive data from at most another K nodes within each fine-grained time period $\tau_{l,n}$, i.e., the number of transmission links going into the node v_i^l must be less than or equal to K. Thus, the following constraint must be satisfied [11]

$$\sum_{\left\{v_j^l:\left(v_j^l, v_i^l\right)\in E_L\right\}} g_{\tau_{l,n}}^{\left(v_j^l, v_i^l\right)} \leq K. \tag{7}$$

B. Transmission Constraints

Denote the transmission capacity of the transmission link $\left(v_i^l, v_j^l\right)$ within the time interval τ_l as $c^{\left(v_i^l, v_j^l\right)}$. Therefore, the transmission capacity of the transmission link $\left(v_i^l, v_j^l\right)$ within the fine-grained time period $\tau_{l,n}$ is $\frac{d_{l,\mathrm{n}}}{\tau} \times c^{\left(v_i^l, v_j^l\right)}$. Furthermore, denote the amount of data transmitted on transmission link $\left(v_i^l, v_j^l\right)$ within the fine-grained time period $\tau_{l,n}$ as $x_{\tau_{l,n}}^{\left(v_i^l, v_j^l\right)}$. If the transmission link $\left(v_i^l, v_j^l\right)$ is established within the fine-grained time period $\tau_{l,n}$, the value of $g_{\tau_{l,n}}^{\left(v_i^l, v_j^l\right)}$ is equal to one and $x_{\tau_{l,n}}^{\left(v_i^l, v_j^l\right)}$ cannot exceed the capacity of that transmission link within the fine-grained time period $\tau_{l,n}$ [11]–[14]. On the contrary, if the transmission link $\left(v_i^l, v_j^l\right)$ is not established within the fine-grained time period $\tau_{l,n}$, the value of $g_{\tau_{l,n}}^{\left(v_i^l, v_j^l\right)}$ is equal to 0 and $x_{\tau_{l,n}}^{\left(v_i^l, v_j^l\right)}$ is 0. Therefore, $x_{\tau_{l,n}}^{\left(v_i^l, v_j^l\right)}$ must satisfy the following constraint [11]–[14]

$$0 \leq x_{\tau_{l,n}}^{\left(v_i^l, v_j^l\right)} \leq \frac{d_{l,\mathrm{n}}}{\tau} \times c^{\left(v_i^l, v_j^l\right)} \times g_{\tau_{l,n}}^{\left(v_i^l, v_j^l\right)}. \tag{8}$$

C. Cache Constraints

Denote the caching capacity of the node v_i as b_i. Furthermore, denote the amount of data stored on caching link $\left(v_i^l, v_i^{l+1}\right)$ coming out of the node v_i^l within the fine-grained time period $\tau_{l,n}$ as $y_{\tau_{l,\mathrm{n}}}^{v_i}$. As the amount of data stored on caching link $\left(v_i^l, v_i^{l+1}\right)$ cannot exceed the caching capacity of the node v_i, $y_{\tau_{l,\mathrm{n}}}^{v_i}$ must satisfy the following constraint [13], [18]

$$\begin{gathered} 0 \leq y_{\tau_{l,\mathrm{n}}}^{v_i} \leq b_i, \\ \text{for } l = 1, 2, \ldots, L; n = 1, 2, \ldots, N_l; n \neq N_L. \end{gathered} \tag{9}$$

D. Flow Conservation Constraints

According to the flow conservation constraint, the total amount of data going into the node v_i^l must be equal to the total amount of data coming out of the node v_i^l. There are four scenarios to consider:

1) Within the fine-grained time period $\tau_{l,n}, n \neq 1$, the node v_i^l can have both incoming transmission links and incoming caching links, as well as both outgoing transmission links and outgoing caching links, as shown in Fig. 3. Furthermore, both the caching link going into this node v_i^l and the caching link coming out of this node v_i^l are within the same fine-grained time period $\tau_{l,n}$, as shown in Fig. 3. Therefore, the flow conservation constraint of the node v_i^l within the fine-grained time period $\tau_{l,n}, n \neq 1$ must satisfy the constraint

$$\begin{aligned} &\sum_{\left\{v_j^l:\left(v_j^l, v_i^l\right)\in E_L\right\}} x_{\tau_{l,n}}^{\left(v_j^l, v_i^l\right)} + y_{\tau_{l,\mathrm{n}-1}}^{v_i} \\ &= \sum_{\left\{v_j^l:\left(v_i^l, v_j^l\right)\in E_L\right\}} x_{\tau_{l,n}}^{\left(v_i^l, v_j^l\right)} + y_{\tau_{l,\mathrm{n}}}^{v_i}, \text{where} \\ &l = 1, 2, \ldots, L; n = 2, 3, \ldots, N_l; i = 1, 2, \ldots, H. \end{aligned} \tag{10}$$

2) Within the fine-grained time period $\tau_{l,1}, l > 1$, the node v_i^l can have both incoming transmission links and incoming caching links, as well as both outgoing transmission links and outgoing caching links, as shown in Fig. 3. However, the caching link going into this node v_i^l is within the fine-grained time period $\tau_{l,n-1}$, while the caching link coming out of this node v_i^l is within the fine-grained time period $\tau_{l,n}$, as shown in Fig. 3. Therefore, the flow conservation constraint of the node v_i^l within the fine-grained time period $\tau_{l,1}, l > 1$ must satisfy the constraint

$$\begin{aligned} &\sum_{\left\{v_j^l:\left(v_j^l, v_i^l\right)\in E_L\right\}} x_{\tau_{l,1}}^{\left(v_j^l, v_i^l\right)} + y_{\tau_{l-1,N_{l-1}}}^{v_i} \\ &= \sum_{\left\{v_j^l:\left(v_i^l, v_j^l\right)\in E_L\right\}} x_{\tau_{l,1}}^{\left(v_i^l, v_j^l\right)} + y_{\tau_{l,1}}^{v_i}, \\ &\text{where } l = 2, 3, \ldots, L; i = 1, 2, \ldots, H. \end{aligned} \tag{11}$$

3) Within the the fine-grained time period $\tau_{1,1}$, the node v_i^l does not have any incoming caching links, which is the case where $\tau_{1,1}$ is the first fine-grained time period in the TEG G, as shown in Fig. 3. Therefore, the flow conservation constraint of the node v_i^l within the fine-grained time period $\tau_{1,1}$ must satisfy the constraint

$$\begin{aligned} &\sum_{\left\{v_j^l:\left(v_j^l, v_i^l\right)\in E_L\right\}} x_{\tau_{1,1}}^{\left(v_j^l, v_i^l\right)} \\ &= \sum_{\left\{v_j^l:\left(v_i^l, v_j^l\right)\in E_L\right\}} x_{\tau_{1,1}}^{\left(v_i^l, v_j^l\right)} + y_{\tau_{1,1}}^{v_i}, \\ &\text{where } i = 1, 2, \ldots, H. \end{aligned} \tag{12}$$

4) Within the fine-grained time period τ_{N,N_L}, the node v_i^l does not have the outgoing caching link, which is the

case where τ_{N,N_L} is the last time period in the TEG G, as shown in Fig. 3. Therefore, the flow conservation constraint of the node v_i^l within the fine-grained time period τ_{N,N_L} must satisfy the constraint

$$\begin{aligned}&\sum_{\left\{v_j^l:\left(v_j^l,v_i^l\right)\in E_L\right\}} x_{\tau_{N,N_L}}^{\left(v_j^l,v_i^l\right)} + y_{\tau_{N,N_L-1}}^{v_i}\\ =&\sum_{\left\{v_j^l:\left(v_i^l,v_j^l\right)\in E_L\right\}} x_{\tau_{N,N_L}}^{\left(v_i^l,v_j^l\right)},\\ &\text{where } i=1,2,\ldots,H.\end{aligned} \tag{13}$$

E. Demand Constraints

The total amount of data that the mission flow coming out of the source node v_1 must be equal to the total amount of data the mission flow going into the destination node v_H [13]. In this case, we have the following constraint

$$\begin{aligned}&\sum_{l=1}^{L}\sum_{n=1}^{N_l}\sum_{\left\{v_j^l:\left(v_1^l,v_j^l\right)\in E_L\right\}} x_{\tau_{l,n}}^{\left(v_1^l,v_j^l\right)}\\ =&\sum_{l=1}^{L}\sum_{n=1}^{N_l}\sum_{\left\{v_j^l:\left(v_j^l,v_H^l\right)\in E_L\right\}} x_{\tau_{l,n}}^{\left(v_j^l,v_H^l\right)}.\end{aligned} \tag{14}$$

F. Maximum Flow Routing Strategy

In this paper, the objective is to maximize the total amount of data that can be transmitted from the source node v_1 to the destination node v_H within the time horizon $[0,T)$ in the TEG G with dynamic link allocation within each time interval under the transceiver constraint, which can be formulated as the following problem

$$\max_{\substack{\{d_{l,n}\}\left\{x_{\tau_{l,n}}^{\left(v_i^l,v_j^l\right)}\right\}\\ \left\{y_{\tau_{l,n}}^{\left(v_i^l,v_j^l\right)}\right\}\left\{g_{\tau_{l,n}}^{\left(v_i^l,v_j^l\right)}\right\}}} \sum_{l=1}^{L}\sum_{n=1}^{N_l}\sum_{\left\{v_j^l:\left(v_1^l,v_j^l\right)\in E_L\right\}} x_{\tau_{l,n}}^{\left(v_i^l,v_j^l\right)} \tag{15a}$$

$$s.t.\ (4)-(14). \tag{15b}$$

As (8) is a quadratic constraint, this max-flow problem is an MIQP problem. However, by introducing a sufficiently large number M, the constraint (8) can be equivalently transformed into two linear constraints [21, Chapter 5]

$$\begin{aligned}&0\le x_{\tau_{l,n}}^{\left(v_i^l,v_j^l\right)}\le \frac{d_{l,\mathrm{n}}}{\tau}\times c^{\left(v_i^l,v_j^l\right)}\times g_{\tau_{l,n}}^{\left(v_i^l,v_j^l\right)}\\ \Leftrightarrow&\begin{cases}0\le x_{\tau_{l,n}}^{\left(v_i^l,v_j^l\right)}\le g_{\tau_{l,n}}^{\left(v_i^l,v_j^l\right)}\times M, & (16a)\\ 0\le x_{\tau_{l,n}}^{\left(v_i^l,v_j^l\right)}\le \dfrac{d_{l,\mathrm{n}}}{\tau}\times c^{\left(v_i^l,v_j^l\right)}. & (16b)\end{cases}\end{aligned}$$

If the transmission link $\left(v_i^l,v_j^l\right)$ is not established within the fine-grained time period $\tau_{l,n}$, the value of $g_{\tau_{l,n}}^{\left(v_i^l,v_j^l\right)}$ is 0, and $x_{\tau_{l,n}}^{\left(v_i^l,v_j^l\right)}=0$. In this case, (16a) is used to meet this constraint. On the contrary, if the link $\left(v_i^l,v_j^l\right)$ is established within time period $\tau_{l,n}$, the value of $g_{\tau_{l,n}}^{\left(v_i^l,v_j^l\right)}$ is equal to one, and $x_{\tau_{l,n}}^{\left(v_i^l,v_j^l\right)}$ cannot exceed the transmission capacity of the link $\left(v_i^l,v_j^l\right)$ within the fine-grained time period $\tau_{l,n}$. In this case, if M is chosen to be greater than $\frac{d_{l,\mathrm{n}}}{\tau}\times c^{\left(v_i^l,v_j^l\right)}$, the constraint (16b) can meet the constraint. Consequently, this MIQP problem is equivalently transformed into an MILP problem, which can be solved by existing algorithms, for example, the Branch and Bound algorithm [19, Chapter 11].

G. Complexity Analysis

Theorem 1. *The time complexity of solving this MILP problem using the Branch and Bound algorithm is approximately upper bounded by* $O((H^2\sum_{l=1}^{L}N_l)^{3.5}2^{H(H-1)\sum_{l=1}^{L}N_l})$.

Proof of Theorem 1: Firstly, we count the number of variables $\{d_{l,n}|1\le l\le L, 1\le n\le N_l\}$. The TEG contains L time intervals, while the l-th time interval contains N_l fine-grained time periods. Hence, there are a total of $\sum_{l=1}^{L}N_l$ fine-grained time periods in the TEG. The total number of variables $\{d_{l,n}|1\le l\le L, 1\le n\le N_l\}$ is also $\sum_{l=1}^{L}N_l$.

Secondly, there is only one variable $x_{\tau_{l,n}}^{\left(v_i^l,v_j^l\right)}$ on each transmission link within each fine-grained time period, the number of variables $\{x_{\tau_{l,n}}^{\left(v_i^l,v_j^l\right)}|(v_i^l,v_j^l)\in E_L\}$ is equal to number of transmission links of all fine-grained time periods. Assuming that there is a transmission link between any two nodes within each fine-grained time period, therefore, the number of transmission links within one fine-grained time period is at most $H(H-1)$. In addition, the TEG contains $\sum_{l=1}^{L}N_l$ fine-grained time periods. Hence, the total number of $\{x_{\tau_{l,n}}^{\left(v_i^l,v_j^l\right)}|(v_i^l,v_j^l)\in E_L\}$ is at most $H(H-1)\sum_{l=1}^{L}N_l$.

Thirdly, we count the number of variables $\{y_{\tau_{l,n}}^{v_i}|1\le l\le L-1\}$ on caching links. As there are H nodes in the SIN, there are H caching links between two consecutive fine-grained time periods. Furthermore, as there are $\sum_{l=1}^{L}N_l$ fine-grained time periods, there are a total of $H(\sum_{l=1}^{L}N_l-1)$ caching links in the TEG. Therefore, the total number of variables $\{y_{\tau_{l,n}}^{v_i}|1\le l\le L-1\}$ is also $H(\sum_{l=1}^{L}N_l-1)$.

Finally, we count the number of binary variables $\{g_{\tau_{l,n}}^{\left(v_i^l,v_j^l\right)}|(v_i^l,v_j^l)\in E_L\}$. As there is only one binary variable $g_{\tau_{l,n}}^{\left(v_i^l,v_j^l\right)}$ on each transmission link within one fine-grained time period, the total number of binary variables $\{g_{\tau_{l,n}}^{\left(v_i^l,v_j^l\right)}|(v_i^l,v_j^l)\in E_L\}$ is at most $H(H-1)\sum_{l=1}^{L}N_l$.

Furthermore, the complexity of solving this MILP problem using branch and bound algorithm mainly depends on the number of binary variables $g_{\tau_{l,n}}^{\left(v_i^l,v_j^l\right)}$, and in the worst case, the complexity increases exponentially with the increase of binary integer variables [22]. As the total number of binary

variables $\{g_{\tau_{l,n}}^{(v_i^l,v_j^l)}|(v_i^l,v_j^l)\in E_L\}$ is $H(H-1)\sum_{l=1}^{L}N_l$, in the worst case, the complexity of solving this MILP problem is equivalent to solving $2^{H(H-1)\sum_{l=1}^{L}N_l}$ linear programming(LP) subproblems [22], [23]. Furthermore, for each LP subproblem, there are $\sum_{l=1}^{L}N_l$ continuous variables $\{d_{l,n}|1\le l\le L, 1\le n\le N_l\}$, at most $H(H-1)\sum_{l=1}^{L}N_l$ continuous variables $\{x_{\tau_{l,n}}^{(v_i^l,v_j^l)}|(v_i^l,v_j^l)\in E_L\}$, and $H(\sum_{l=1}^{L}N_l-1)$ continuous variables $\{y_{\tau_{l,n}}^{v_i}|1\le l\le L-1\}$. Hence, there are at most a total of $(H^2+1)\sum_{l=1}^{L}N_l-H$ continuous variables, the complexity of solving each LP subproblem is upper bounded by $O((H^2+1)\sum_{l=1}^{L}N_l-H)^{3.5}$ [24]. Therefore, the time complexity to solve this MILP problem is upper bounded by $O(((H^2+1)\sum_{l=1}^{L}N_l-H)^{3.5}2^{H(H-1)\sum_{l=1}^{L}N_l})\approx O((H^2\sum_{l=1}^{L}N_l)^{3.5}2^{H(H-1)\sum_{l=1}^{L}N_l})$. ■

IV. Simulation Results

In this section, simulation results are provided to demonstrate the performance of the proposed dynamic link allocation under the transceiver constraint. The network topology is obtained through the Satellite Tool Kit (STK) 9.2.3 software. The constraint and the maximal flow objective function are described using YALMIP in MATLAB R2017b. Furthermore, the CPLEX 12.8 is invoked in MATLAB R2017b to solve the MILP using the Branch nd Bound algorithm. In our simulation, a system consisting of eight satellites selected from the IRIDIUM system and one ground station located in Xi'an, China ($34.27°$N, $108.93°$E) is used. All satellites are fixed at an altitude of 780 km and an inclination of $86.4°$. In addition, the number of transceivers is assumed to be $K=1$ for simplification. The simulation time interval length τ is set to be 20 minutes, while the inter-satellite link rate range is set to $10\sim 40$ Mbps, which follows the uniform distribution, and the satellite-to-ground link rate is set to $20\sim 100$ Mbps, which also follows the uniform distribution. Furthermore, $N_1=N_2=\ldots=N_L=N$ is assumed in the simulation.

In Fig. 4, the maximum flow versus the time horizon T is plotted with 20 Gbit cache capacity for each satellite, where N indicates that the number of fine-grained time periods within each time interval. As can be seen from Fig. 4, the maximum flow for $N=2$ and $N=3$ is higher than that for $N=1$. Furthermore, the maximum flow almost always increases with the growth of the time horizon T. As T grows, the scale of the network topology expands, and the number of transmission links increases, so the maximum flow increases. However, for any given N, the maximum flow is the same for $T=3$ and $T=4$ in Fig. 4. The reason is that during the duration from $T=3$ to $T=4$, no satellite is connected to the ground station in the simulated topology; hence, no data is transmitted to the ground station. Moreover, the performance gain of $N=2$ over $N=1$ is about 24% for $T=2$. Furthermore, the similar performance can be achieved for both $N=2$ and $N=3$.

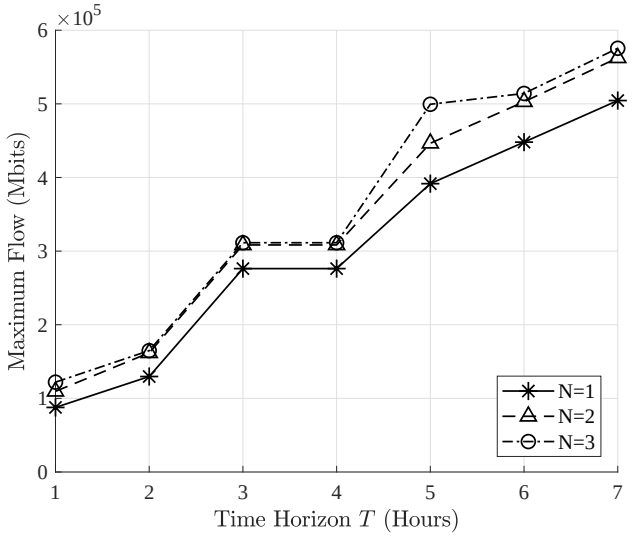

Fig. 4. The maximum flow versus the time horizon T.

In Fig. 5, the maximum flow versus the cache capacity is plotted for time horizon $T=2$, where N indicates that the number of fine-grained time periods within each time interval. Furthermore, the simulations are performed for three different configurations of transmission link capacities, where the performance gain of $N=2$ over $N=1$ is 12%, 16%, and 24% respectively. As seen from Fig. 5, the maximum flow for $N=2$ is higher than that for $N=1$, which is the fixed link allocation strategy within each time interval. Furthermore, for small to moderate cache capacity, the maximum flow increases as the cache capacity increases, because more data can be buffered and transmitted to the destination node in later fine-grained time periods. However, as the cache capacity continues to increase, the maximum flow reaches an upper bound. The reason is that the maximum flow is limited by the capacity of transmission links in this case, and the maximum flow no longer increases with the increase of the cache capacity.

V. Conclusion

In this paper, we proposed a maximum flow routing strategy for SINs by joint optimization of the fine-grained time period duration and the dynamic link allocation within each time interval under a constraint on the number of transceivers. This problem was first formulated as an MIQP and then equivalently transformed into an MILP. The latter can be efficiently solved by existing methods, such as the Branch and Bound algorithm. Simulation results show that the proposed joint optimization of the fine-grained time period duration and the dynamic link allocation within each time interval can significantly outperform the fixed link allocation strategy within one time interval and achieve 12% performance gain.

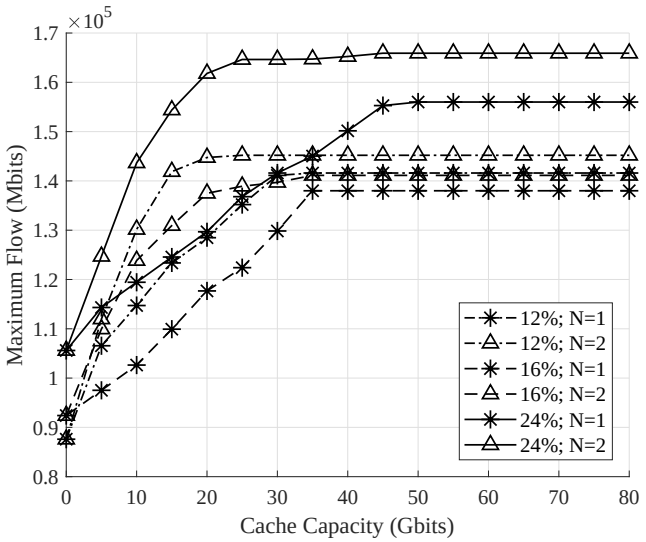

Fig. 5. The maximum flow versus the cache capacity.

REFERENCES

[1] X. Zhang, L. Zhu, T. Li, Y. Xia, and W. Zhuang, "Multiple-user transmission in space information networks: Architecture and key techniques," *IEEE Wireless Communications*, vol. 26, no. 2, pp. 17–23, 2019.

[2] H. Lu, Y. Gui, X. Jiang, F. Wu, and C. W. Chen, "Compressed robust transmission for remote sensing services in space information networks," *IEEE Wireless Communications*, vol. 26, no. 2, pp. 46–54, 2019.

[3] M. Bacco, L. Boero, P. Cassara, M. Colucci, A. Gotta, M. Marchese, and F. Patrone, "IoT applications and services in space information networks," *IEEE Wireless Communications*, vol. 26, no. 2, pp. 31–37, 2019.

[4] J. Mukherjee and B. Ramamurthy, "Communication technologies and architectures for space network and interplanetary internet," *IEEE Communications Survey & Tutorials*, vol. 15, no. 2, pp. 881–897, 2013.

[5] M. Sheng, D. Zhou, R. Liu, Y. Wang, and J. Li, "Resource mobility in space information networks: Opportunities, challenges, and approaches," *IEEE Network*, vol. 33, no. 1, pp. 128–135, 2019.

[6] D. Chen, W. Wang, and T. Jiang, "New multicarrier modulation for satellite-ground transmission in space information networks," *IEEE Network*, vol. 34, no. 1, pp. 101–107, 2020.

[7] Q. Yu, W. Meng, M. Yang, L. Zheng, and Z. Zhang, "Virtual multi-beamforming for distributed satellite clusters in space information networks," *IEEE Wireless Communications*, vol. 23, no. 1, pp. 95–101, 2016.

[8] M. Sheng, Y. Wang, J. Li, R. Liu, D. Zhou, and L. He, "Toward a flexible and reconfigurable broadband satellite network: Resource management architecture and strategies," *IEEE Wireless Communications*, vol. 24, no. 4, pp. 127–133, 2017.

[9] T. Zhang, J. Li, H. Li, S. Zhang, P. Wang, and H. Shen, "Application of time-varying graph theory over the space information networks," *IEEE Network*, vol. 34, no. 2, pp. 179–185, 2020.

[10] T. Zhang, H. Li, S. Zhang, J. Li, and H. Shen, "STAG-based QoS support routing strategy for multiple missions over the satellite networks," *IEEE Transactions on Communications*, vol. 67, no. 10, pp. 6912–6924, 2019.

[11] Y. Wang, M. Sheng, W. Zhuang, S. Zhang, N. Zhang, R. Liu, and J. Li, "Multi-resource coordinate scheduling for earth observation in space information networks," *IEEE Journal on Selected Areas in Communications*, vol. 36, no. 2, pp. 268–279, 2018.

[12] T. Zhang, H. Li, J. Li, S. Zhang, and H. Shen, "A dynamic combined flow algorithm for the two-commodity max-flow problem over delay-tolerant networks," *IEEE Transactions on Wireless Communications*, vol. 17, no. 12, pp. 7879–7893, 2018.

[13] H. Yang, W. Liu, H. Li, and J. Li, "Maximum flow routing strategy for space information network with service function constraints," *IEEE Transactions on Wireless Communications*, vol. 21, no. 5, pp. 2909–2923, 2022.

[14] P. Wang, X. Zhang, S. Zhang, H. Li, and T. Zhang, "Time-expanded graph-based resource allocation over the satellite networks," *IEEE Wireless Communications Letters*, vol. 8, no. 2, pp. 360–363, 2019.

[15] Q. Yu, J. Wang, and L. Bai, "Architecture and critical technologies of space information networks," *Journal of Communications & Information Networks*, vol. 1, no. 3, pp. 1–9, 2016.

[16] J. A. Fraire and J. M. Finochietto, "Design challenges in contact plans for disruption-tolerant satellite networks," *IEEE Communications Magazine*, vol. 53, no. 5, pp. 163–169, 2015.

[17] D. Zhou, M. Sheng, X. Wang, C. Xu, R. Liu, and J. Li, "Mission aware contact plan design in resource-limited small satellite networks," *IEEE Transactions on Communications*, vol. 65, no. 6, pp. 2451–2466, 2017.

[18] D. Zhou, M. Sheng, R. Liu, Y. Wang, and J. Li, "Channel-aware mission scheduling in broadband data relay satellite networks," *IEEE Journal on Selected Areas in Communications*, vol. 36, no. 5, pp. 1052–1064, 2018.

[19] D. Chen, R. Batson, and Y. Dang, *Applied integer programming: modeling and solution*. John Wiley & Sons, 2011.

[20] T. Zhang, S. Deng, H. Li, R. Hou, and H. Zhang, "A maximum flow algorithm for buffer-limited delay tolerant networks," *Journal of Communications and Information Networks*, vol. 2, no. 3, pp. 52–60, 2017.

[21] R. A. Sarker and C. S. Newton, *Optimization modelling: a practical approach*. CRC press, 2007.

[22] D. R. Morrison, S. H. Jacobson, J. J. Sauppe, and E. C. Sewell, "Branch-and-bound algorithms: A survey of recent advances in searching, branching, and pruning," *Discrete Optimization*, vol. 19, pp. 79–102, 2016.

[23] S. University, "Branch and bound methods," https://stanford.edu/class/ee364b/lectures/bb_slides.pdf.

[24] T. H. Cormen, C. E. Leiserson, R. L. Rivest, and C. Stein, *Introduction to algorithms*. MIT press, 2009.